Frequency control in an islanded hybrid microgrid using frequency response analysis tools

Mohsen Aryan Nezhad, Hassan Bevrani

Published (to be published) in: ***IET Renewable Power Generation***

(Expected) publication date: **2017**

Citation format for published version:

Mohsen Aryan Nezhad, Hassan Bevrani. (2017, October 21). Frequency control in an islanded hybrid microgrid using frequency response analysis tools. *IET Renewable Power Generation, 12*(2), 227-243.

IET Renewable Power Generation

Research Article

IET Journals
The Institution of Engineering and Technology

Frequency control in an islanded hybrid microgrid using frequency response analysis tools

ISSN 1752-1416
Received on 3rd April 2017
Revised 17th October 2017
Accepted on 21st October 2017
E-First on 23rd November 2017
doi: 10.1049/iet-rpg.2017.0227
www.ietdl.org

Mohsen Aryan Nezhad[1] ✉, *Hassan Bevrani*[1]

[1]*Smart/Micro Grids Research Center, Department of Electrical & Computer Engineering, University of Kurdistan, Sanandaj, Iran*
✉ *E-mail: m.aryannezhad@eng.uok.ac.ir*

Abstract: A hybrid microgrid has numerous decentralised control loops. Therefore, coordination among hybrid microgrid subsystems with desired performance is essential. This study presents a practical control approach for efficient tuning of proportional–integral (PI) controllers and leads compensators in islanded hybrid microgrids. This method is based on the frequency response characteristic and root-locus trajectory. It is used to minimise the frequency deviations of an AC hybrid microgrid. The presented well-tuned controllers are tuned based on droop mechanism, and coordination among hybrid microgrid subsystems with desired damping coefficient and stability margin. Then, the system performance is analysed under several disturbances. The results are compared with PI controllers tuned by Ziegler–Nichols method. As well, the robustness of the proposed approach in a wide range of parameter changes is investigated. Eigenvalue analysis and simulation results show that the minimum frequency deviations and desired relative stability of the hybrid microgrid subsystems are achieved by the proposed controllers. To show generality and efficiency of the proposed approach, the presented method is applied to a different hybrid microgrid model used in the literature. For this purpose, in order to control the frequency deviations in the stand-alone mode, presented well-tuned controller is compared with intelligent fuzzy and particle swarm optimisation-fuzzy controllers.

Nomenclature

K_P	proportional coefficient
K_I	integral coefficient
K_D	derivative coefficient
T_o	lead compensator zero
ζ	damping coefficient
ω_n	natural frequency
ω_c	gain crossover frequency

1 Introduction

Conventional methods for generation, transmission, and distribution of the electrical energy cause the extensive waste of energy, loss of resources, and impressive negative effects on the environmental pollutions. The RESs such as phototvoltaic (PV) and wind turbine (WT) produce low or no carbon dioxide and other chemical pollutants. Hence, they have a minimal effect on the environment and human health. In order to avoid environmental problems and to ensure energy security for urban and rural societies, the distributed energy resources (DER) extension is inevitable [1].

By decentralised generation, the required electrical energy for the remote areas can be provided with more efficiency and high reliability [2]. This idea was introduced in 1998 by consortium for electric reliability technology solutions (CERTS) [3]. The CERTS was founded to investigate, develop, and enhance reliability and efficiency of the electric power system using DER technologies [4]. The CERTS introduced the DER as the integration of loads and microsources (MSs) operating as a single electric system [5].

The variable renewable energy (VRE), such as solar radiation or wind speed, is a renewable energy source that is non-dispatchable because of its intermittent characteristic [6]. The non-dispatchable power providers are intermittent power generators which cannot be controlled by operators to meet the load demand variations [7]. Therefore, such renewable technologies are generally integrated alongside the conventional power provider, such as diesel generator (DG) [8]. As well, the modern technologies like the energy storage systems and fuel cell (FC) power plants are generally used in the hybrid microgrid (HMG) to enhance load-following capability [9]. This combination of different types of power providers creates the HMG [10]. So, the HMG combines the advantages of renewable, conventional, and modern power providers [11]. When the non-dispatchable power is unavailable, the HMG can always count on the other power providers to supply loads [12]. Hence, the HMG is appropriate as a stand-alone system to provide electrical energy in remote and rural areas with high reliability [13].

The FC has many specifications that make it appropriate for the HMG [14]. It is highly reliable, operates quietly, has the simple maintenance, and produces clean power with higher efficiency than DG [14]. In particular, the FC is an electrochemical device that converts the chemical energy into electricity, directly [15]. It is a new technology and exciting industrial area for large-scale power production [16]. Therefore, the FC is widely used for stationary and mobile applications and currently is under serious development by numerous manufacturers [16]. However, the load fluctuations can cause unstable operation of the FC power plant [16]. Therefore, the hybrid system needs an energy storage system with high-power density, like a ultracapcator (UC) bank, to respond to the load fluctuations, quickly [17]. The UC bank controls DC-link voltage and the frequency of the HMG under serious disturbances [18]. It can supply a huge amount of energy in a short time, which cannot be provided by the DG, FC, and WT [19]. Owing to its benefits, the UC is under development for different purposes.

Recently, many investigations have been made to study control challenges and modelling of the HMGs. In [5], a particle swarm optimisation (PSO)-based fuzzy approach is presented to improve the frequency stability of the islanded hybrid system consisting of the DG, FC, PV, WT, flywheel energy storage system, and battery. The developed PSO-fuzzy-based controller is designed in the DG/FC control loop. Then, the results are compared with the conventional proportional–integral (PI) controller tuned by Ziegler–Nichols (ZN) method. In [10], a neuro-fuzzy controller is designed for power management of PV unit in the HMG. The system frequency variation is used as a feedback signal for the frequency regulation. The presented controller efficiently damps the frequency deviations in all considered scenarios. In [19], the PSO and genetic algorithm (GA)-based loop shaping of H-infinity controllers in the FC control loop are presented. These controllers

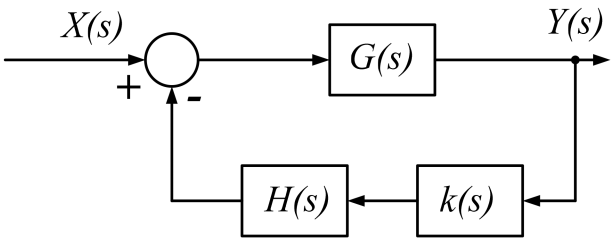

Fig. 1 *Standard closed-loop system*

are used to minimise the load frequency deviations. Next, the results are compared with conventional PI controllers. In [20], a new fuzzy logic pitch controller is designed to reduce power fluctuations of the WT during the microgrid (MG) islanded mode. Then, the results are compared with a conventional controller. In [21], the fuzzy control technique is used to perform power sharing in a hybrid system consisting of the FC, PV, and battery. The obtained results show that the presented control technique keeps the power balancing in the hybrid system, effectively. In [22], the PSO-based Sugeno fuzzy logic controller for PV system is designed to control the frequency deviations of a stand-alone system. The membership functions and control rules of the Sugeno fuzzy controller are tuned by PSO method to reduce the system frequency fluctuations.

The main idea for using of such complex and intelligent controllers is providing of desired performance, such as improving system stability, overshoot/undershoot, and settling time. Then, to demonstrate the intricate controller performance, the obtained results are compared with conventional controllers. The main control drawbacks of the used approaches in the reviewed references can be summarised as follows:

i. The reported conventional controllers presented in the mentioned works suffer from a poor performance in terms of stability, settling time, and overshoot/undershoot due to inefficient tuning methods.
ii. The presented eigenvalue analysis shows that the DG unit has the low damping coefficient in the HMG, and an effective control-based approach for enhancing of the DG stability margin is not proposed.
iii. The mentioned studies are focused on a particular section of the hybrid system, and coordination among decentralised power providers is not considered.
iv. In remote and rural areas, the complex and high-order controllers often cannot be implemented due to performance/maintenance cost, and design complication. In addition, experts cannot be easily available in such areas for tuning, operation, and maintenance of complex controllers.

To cover the mentioned control issues, a set of required control conditions for each distributed generation (DIG) is considered and evaluated to provide system coordination, robustness, and stability with the fast response. As well, a simple-structured compensator is obtained to enhance DG damping coefficient. Using simple controllers to satisfy the mentioned requirements is more attractive. In addition, following any change in the hybrid system structure over the time, the set point of the simple controller can be easily changed to the new operating point condition.

In this direction, the present work addresses efficient tuning of the simple PI controller and lead compensator (LC) based on the system root-locus and frequency response techniques. Eigenvalue analysis confirms that the LC designed in the DG governor loop enhances the DG stability margin and improves the system damping. In addition, the well-tuned controllers can appropriately provide coordinated frequency control with desired robustness, stability, settling time, and undershoot in the face of system parameter perturbations and random/step disturbances.

To confirm generality and efficiency of the proposed methodology, this technique is applied to the given HMG presented in [5]. Then, the obtained results are compared with the outcomes of the fuzzy and PSO/fuzzy-based approaches. The comparison among the PI/LC, fuzzy, and PSO/fuzzy controllers shows that the designed PI/LC provides a smaller undershoot with lower settling time than the intelligent controllers. This is obtained because the PI/LC is tuned based on desired relative stability, the proper damping coefficient of the HMG dominant poles, and coordination among HMG subsystems.

The presented control approach regulates the load frequency on the nominal value with a fast response. This response is obtained because designed controllers are tuned to coordinate all HMG subsystems and to provide desired relative stability and proper damping coefficient. While in the mentioned references, only the overall performance of the hybrid system is investigated and decentralised control loops are not coordinated to reduce the HMG frequency deviations. Unlike the intelligent and complex controllers, the proposed controllers are simple structure and user friendly that their set points can be easily changed to the new condition for every change in the HMG structure. Therefore, the simplicity, flexibility, coordination among HMG control loops, better control performance, and lower operation/maintenance costs can significantly increase the feasibility of the presented tuning approach for the HMG frequency control.

This paper is organised as follows: Section 2 illustrates mathematical descriptions and the required control conditions for the effective tuning of the conventional controllers and compensators. In Section 3, dynamic models of the WT, FC, DG, and UC are presented. The proposed control strategy is discussed in Section 4. Tuning of the well-tuned controllers based on proposed control strategy is presented in Section 5. Simulation studies are given in Section 6. Finally, the paper is concluded in Section 7.

2 Closed-loop characteristic equation

The root-locus method is a graphical technique to demonstrate the effect of the system gain variation on the roots of a closed-loop system. The standard model of a closed-loop control system is represented in Fig. 1.

In Fig. 1, $G(s)$, $H(s)$, and $k(s)$ are the feedforward, feedback, and controller transfer functions, respectively. Interested readers can find more details about the root-locus analysis, and the frequency response characteristic in [23–26].

According to the closed-loop equation, the PI or PI–derivative (PID) controllers can be designed so that the system characteristic equation performs desired damping coefficient, ζ, and safe gain margin (GM) and phase margin (PM) as

$$1 + k(s)G(s)H(s) = 1 + \underbrace{\left(K_{\mathrm{P}} + \frac{K_{\mathrm{I}}}{s}\right)}_{\mathrm{PI}(s)} \cdot \left(\frac{s^n + a_{n-1}s^{n-1} + \cdots + a_0}{s^m + b_{m-1}s^{m-1} + \cdots + b_0}\right) = 0 \tag{1}$$

$$1 + k(s)G(s)H(s) = 1 + \underbrace{\left(\left(K_{\mathrm{P}} + \frac{K_{\mathrm{I}}}{s}\right).(s + T_{\mathrm{o}})\right)}_{\mathrm{PID}(s)} \cdot \left(\frac{s^n + a_{n-1}s^{n-1} + \cdots + a_0}{s^m + b_{m-1}s^{m-1} + \cdots + b_0}\right) = 0 \tag{2}$$

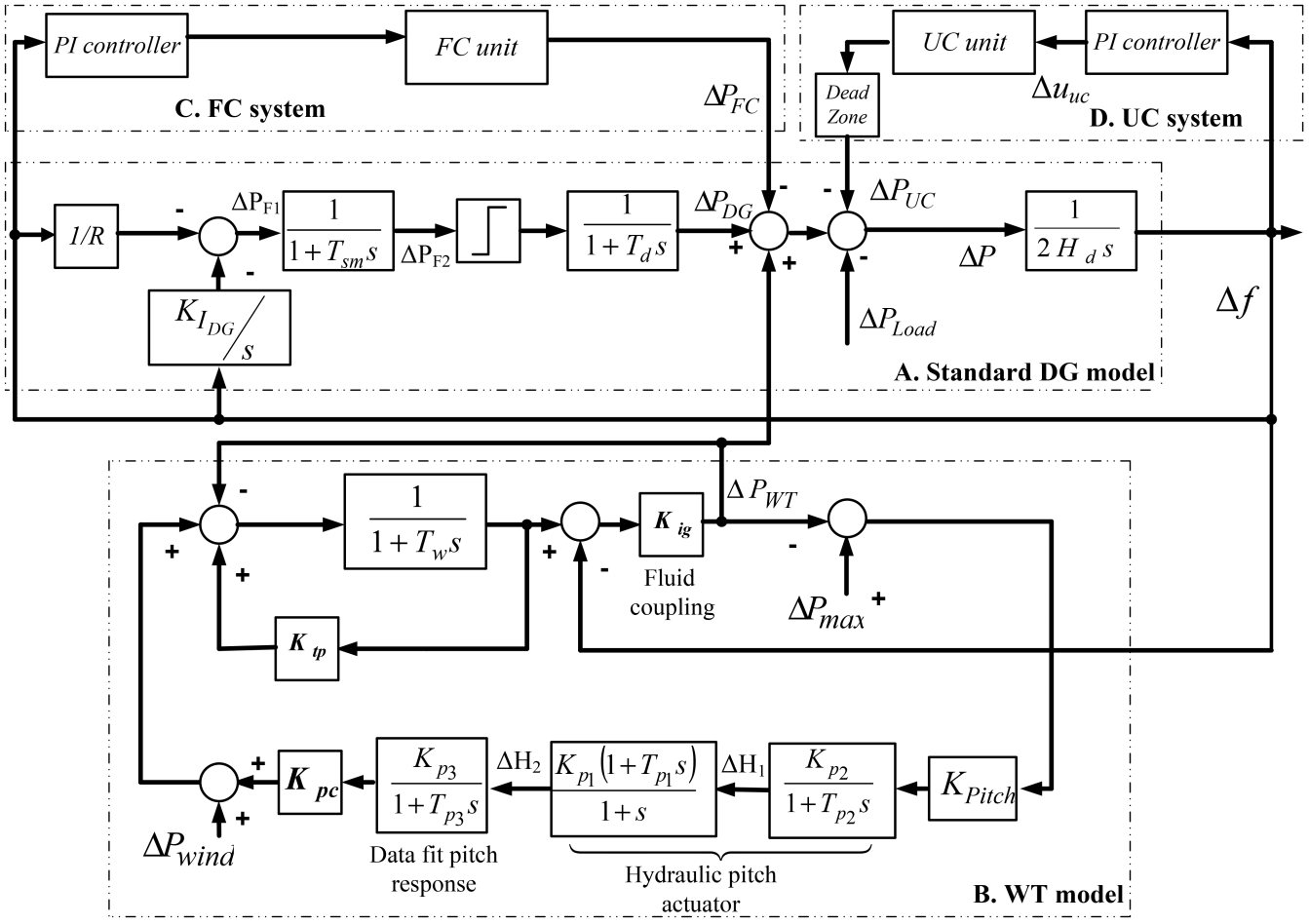

Fig. 2 *Block diagram of the hybrid system*

The ζ between 0.4 and 0.7 provides a good system response with proper overshoot/undershoot and settling time, and PM ≥ 30° with GM ≥ 6 dB ensure that system remains stable, despite changes in the system parameters [23]. Those proper values ensure the required stability and performance of a minimum-phase system even if the open-loop gain and system parameters change around their nominal values [23]. Therefore, the mentioned values for ζ, PM, and GM provide suitable conditions for efficient tuning of PI controllers and compensators in a minimum-phase system.

3 HMG modelling

The hybrid system includes the following subsystems: DG, FC unit, WT, and UC model. This block diagram of the HMG model is shown in Fig. 2. Since the HMG works at low frequency (60 Hz) and the DG, FC, and WT have the slow nature and mechanism, it is interesting to investigate the dynamic response of the hybrid system at low frequencies. To remove effects of high-frequency components created by the inverter switching on the HMG performance, the lowpass filters are also used at the output terminals of the FC and UC inverters [6]. Therefore, the HMG model shown in Fig. 2 is presented to investigate the frequency control and dynamic behaviour of the hybrid system at low frequencies [6, 27, 28]. Interested readers can find more details about modelling, dynamic system characteristic, and accurate model assessment and verification of the presented HMG in [26–33]. The parameter values and rating of the HMG subsystems are given in the Appendix [5, 19, 27, 33–37]. Several microgrid modelling approaches are also discussed in [38, 39].

3.1 DG model

In Fig. 2, the standard model of the DG unit is presented in block A [27]. This model illustrates the dynamic behaviour of the DG set. The input of the DG is the load changes, and output is the frequency deviations [27]. The diesel engine and valve actuator are modelled as the first-order transfer functions with time constants of T_{sm} and T_d, respectively. Inertia is shown by H_d and the governor consists of droop constant (R), and the integral controller [27]. For an appropriate response, the DG droop value is chosen between 3 and 7%. This limited range avoids unacceptable frequency error in the steady-state situations [27]. The integral controller in the DG feedback loop removes this steady-state error. However, this issue decreases the DG stability margin and creates more oscillations in the output frequency deviations [27].

3.2 WT model

The power generation of WT depends on wind speed V (m/s), and it changes as a cubic function [19]. The mechanical power of the WT is given by

$$P_{\mathrm{WT}} = \frac{1}{2}\rho A_{\mathrm{r}} C_{\mathrm{p}} V^3 \tag{3}$$

where ρ is the density of air (kg/m^3), A_{r} is the blade swept area (m^2), C_{p} is a coefficient that changes as a function of tip speed ratio (λ) and pitch angle of blade (β) [19]. The WT dynamic model includes low-speed shaft, high-speed shaft, hydraulic pitch control, and fluid coupling transfer functions as shown in block B of Fig. 2 [19, 25].

3.3 FC model

The FC system is shown in block C of Fig. 2. It consists of a fuel tank, an inverter for changing DC to AC voltage, and an interconnection [5]. It can be modelled as a third-order characteristic with time constants of T_{ln}, T_{IC}, and T_{fc} [5]

$$\mathrm{FC}(s) = \frac{1}{(1+T_{\mathrm{IC}}s)(1+T_{\mathrm{ln}}s)(1+T_{\mathrm{fc}}s)} \tag{4}$$

3.4 UC model

The UC system is shown in block D of Fig. 2. It can track transient load changes, immediately. It causes that conventional energy providers work at the constant output or change the generation level, slowly. The UC is modelled as a first-order transfer function with time constant of T_{UC} [19] as follows:

$$UC(s) = \frac{1}{1 + T_{UC}s} \tag{5}$$

4 Proposed control strategy

The efficient tuning of the PI/LC is based on control requirements mentioned in Section 2. The target is to select the controller parameters so that the HMG dynamic model has a safe GM and PM, with desired damping coefficient. To enhance the PM and achieve proper damping, the LC in series with PI controller can be designed. This LC is used to place the dominant poles of the system closed-loop on a suitable location, and improve the PM of the system, effectively. This combination creates a PID controller that can be formulated as

$$PID(s) = (s + T_o)\left(\frac{K_I}{s} + K_P\right) = \underbrace{(K_I + T_oK_P)}_{K'_P} + \underbrace{\frac{K_IT_o}{s}}_{K'_I/s} + \underbrace{K_Ps}_{K'_Ds} \tag{6}$$

where $(s + T_o)$ is an LC that is used in series with a PI controller. In addition, K'_P, K'_I, K'_D are the PID coefficients that are obtained based on the PI and LC parameters.

5 Tuning of the well-tuned controllers

5.1 Performance improvement of DG unit

A DG unit can directly change the generation level in a hybrid system. Therefore, improvement of DG dynamic performance has a positive effect on the load-frequency profile. For this purpose, the standard model of DG unit is considered as presented in Fig. 2 (block A). According to the locus of DG unit, the effect of the governor droop on the system dynamic is plotted in Fig. 3*a*.

In Fig. 3*a*, the root-locus of DG unit is shown with the DG droop as a variable parameter. It shows that the damping coefficient of DG increases with decreasing the gain value $(1/R)$. In this case, one can select the desired droop between 3 and 7%. For an appropriate DG response, the droop value is fixed at $R = 5\%$. For this value of droop, the DG dynamic behaviour is influenced by a pair of lightly damped complex poles. The open-loop bode plot (Fig. 3*a*) shows that the GM and PM are larger than 6 dB and 30°. For removing of steady-state error, an integral controller with $K_{I_{DG}} = 8$ is also added to the feedback loop.

However, by adding the DG droop and integral controller in the DG feedback loop, the order of the open-loop system increases. As shown in Fig. 3*b*, the PM, GM, and damping coefficient reduce to 14.3°, 8.21 dB, and 0.129, respectively. So, the new PM and ζ are lower than the required values. The gain crossover frequency for PM = 14.3 is about $\omega_c = 3.37$ rad/s. To increase the PM before crossover frequency, an LC with $s = -1$ can be added to the feedback loop. It causes that the open-loop pole of the integral controller at $s = 0$ tends to be added zero at $s = -1$. The bode plot and root-locus of compensated DG are presented in Figs. 4*a* and *b*. The designed LC provides a significant improvement in the ζ, PM, and GM of the system. The root-locus of the DG unit, shown in Fig. 4*a*, confirms that its dynamic behaviour is influenced by a pair of high damped complex poles with $\zeta = 0.6$. The compensated system has an infinite GM, with PM = 63.1°, as illustrated in Fig. 4*b*.

The combination of the DG droop, integral controller, and LC performs a dynamic model as

$$PID_{DG}(s) = \left(20 + \left(\frac{8}{s}\right)\right) \times (s + 1) = \frac{20s^2 + 28s + 8}{s}$$

This is equal to the transfer function of a PID controller as $28 + 20s + (8/s)$ with $K'_{P_{DG}} = 28$, $K'_{I_{DG}} = 8$, and $K'_{D_{DG}} = 20$. In this case, the total DG droop with the LC in the feedback loop is equal to $(1/K'_{P_{DG}}) \times 100 = (1/28) \times 100 = 3.57\%$. This droop value is 1.43% lower than DG droop value with a PI controller in the feedback loop. Therefore, the designed series LC decreases the DG droop value, improves the system damping, and increases the DG stability margin.

5.2 Contribution of WT with DG unit

In this section, an AC-WT participates with the DG unit. Such a new configuration needs coordination between DG and WT units. For a system with several transfer functions and intricate configuration, the state-space equations can be extracted using *linmod* command in Matlab software. With indicating the input and output of the system in Matlab/Simulink environment, this command directly extracts the state-space equations between identified input and output. For standard configuration presented in Fig. 1, it is required to determine the inputs and outputs of the $G(s)$ and $H(s)$. Then, the required state-space equations for the feedforward and feedback transfer functions can be obtained using the mentioned command.

As shown in Fig. 5, the signal of frequency deviations is directly applied to the WT pitch loop. Therefore, WT contribution for the HMG frequency control requires coordination between the WT pitch loop and DG governor.

The gain in the pitch loop, K_{Pitch}, acts as a proportional controller. From the open-loop transfer functions of WT system, the pitch loop gain of $K_{Pitch} = 272$ can create GM = 36.3 dB, and infinite PM with $\zeta = 0.9$. The pitch loop of WT has a slow mechanism due to the slow nature of the hydraulic system and mechanical moving parts. Therefore, DG controller tunes the overall damping of the WT/DG system to the desired value and accelerates the system response. To build a standard type of the closed-loop configuration as presented in Fig. 1, it is required to obtain feedforward and feedback transfer functions of the overall system. The feedback transfer function of WT/DG system is the DG governor loop, and the remaining of WT/DG model is a feedforward transfer function. Using the *linmod* command for calculation of the required state-space equations, the root-locus and bode plot of DG/WT are obtained as shown in Figs. 6*a* and *b*.

The proportional gain equal to 23.7 in the DG feedback loop gives the DG droop about $R = 4.22\%$. This droop value is within the nominal DG droop range. For removing of steady-state error, an integral controller with $K_{I_{DG}} = 4$ is added to the DG feedback loop. Once the PI controller is added to the feedback loop, the GM = 10.5 dB, PM = 23°, and $\xi = 0.2$ are achieved. For another integrator coefficient of $K_{I_{DG}} = 1$, the GM is equal to 11 dB, PM = 25.1 and $\xi = 0.21$. In both cases, the PM and ξ are lower than the minimum control requirements. Hence, it is needed to compensate the system with an LC in the feedback loop of the DG unit.

As shown in Fig. 6*a*, two branches that leave the stable area to unstable zone need the positive phase to stay in the stable area. This issue enhances the system damping. For this purpose, an LC with $s = -1.25$ is added to the feedback loop. So, the root-locus of the added zero in $s = -1.25$ and an open-loop pole in $s = -1.148$ locates on the real axis. This added zero creates a closed-loop pole in $s = -1.237$. In this case, the root-locus and bode plot of the compensated system are shown in Figs. 7*a* and *b*. Since the added zero is near the origin, it creates the PM = 61.5° with GM = Inf (dB). In addition, the dominant poles of the system have $\zeta = 0.58$. Therefore, this LC provides the required conditions for the GM, PM, and ζ.

So, the required PI/LC in the DG feedback loop is

$$\left(23.7 + \left(\frac{4}{s}\right)\right)(s + 1.25) = \frac{23.7s^2 + 33.6s + 5}{s}$$

It is equivalent to a PID controller with $K'_{P_{DG}} = 33.6$, $K'_{I_{DG}} = 5$, and $K'_{D_{DG}} = 23.7$ $(PID_{DG}(s) = 33.6 + 23.7s + (5/s))$. In this case, the

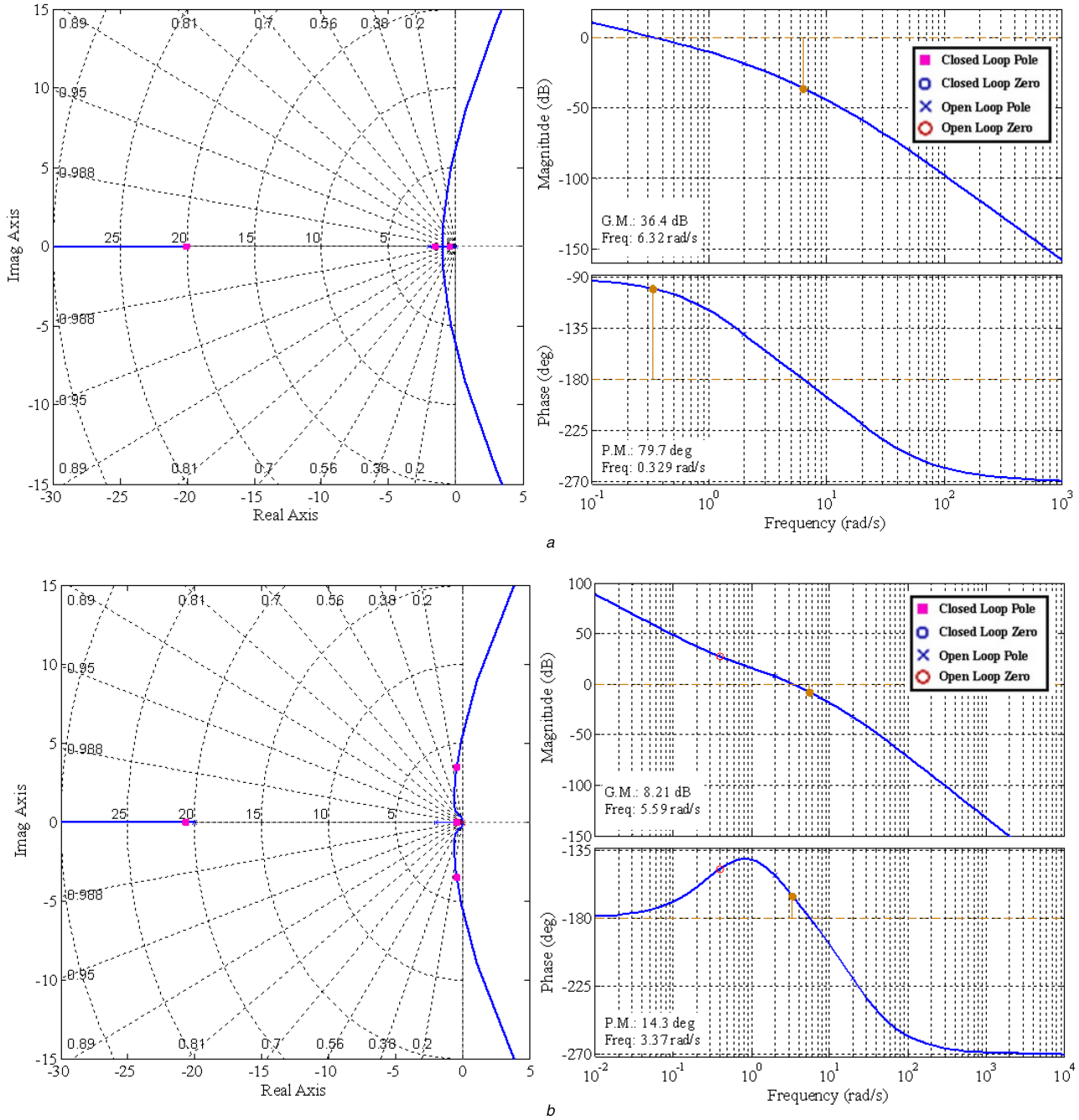

Fig. 3 *Root-locus and bode plot of the DG unit*
(a) Without PI controller,
(b) With PI controller

DG droop is about 3%. Therefore, designed series LC provides the large stability margin for DG unit with lower droop value.

5.3 Participation of FC with DG/WT system

To design the FC controller, the feedforward and feedback transfer functions of the overall system should be obtained. These functions are used to build a standard type of closed-loop configuration as presented in Fig. 1. The WT/DG system is the feedforward transfer function, and the feedback is the FC transfer function that is formulated in (4). Using the *linmod* command to calculate the required transfer functions, the bode-plot and root-locus of the hybrid system are plotted in Figs. 8*a* and *b*.

As plotted in Fig. 8*a*, the DG/WT/FC system has two dominant open-loop poles at -8.71 ± 16j. In this case, the GM = 43.2 dB, and the PM is infinite. According to (1), the PI controller of the FC unit can be formulated as

$$\mathrm{PI}_{\mathrm{FC}}(s) = K_{P_{\mathrm{FC}}} + \frac{K_{I_{\mathrm{FC}}}}{s} = K_{I_{\mathrm{FC}}}\left(\frac{1 + T_{\mathrm{FC}}s}{s}\right)$$

where $K_{P_{\mathrm{FC}}} = K_{I_{\mathrm{FC}}}T_{\mathrm{FC}}$. The gain value $K_{P_{\mathrm{FC}}} = 3$ gives desired damping coefficient, $\zeta = 0.452$. To locate the root-locus of the closed-loop pole on the real axis, the open-loop zero of PI controller $(1 + T_{\mathrm{FC}}s)$ is selected in $s = -0.6$. It is on the left side of the open-loop pole in $s = -0.171$. Thus, the added zero gives $T_{\mathrm{FC}} = 1.667$. So, the locus of the open-loop pole at $s = -0.171$ tends to the added zero at $s = -0.6$ on the real axis. Therefore, the PI controller for the FC unit is obtained as: $\mathrm{PI}_{\mathrm{FC}}(s) = 1.8 \times (((1 + 1.667s)/s))$ with $K_{P_{\mathrm{FC}}} = 3$, and $K_{I_{\mathrm{FC}}} = 1.8$.

In this case, the root-locus and bode plot of the open-loop DG/WT/FC system with the obtained PI controller in the FC loop can be plotted as shown in Figs. 8*c* and *d*. As illustrated in Figs. 8*c* and *d*, the ζ, GM, and PM of the open-loop system are 0.452, 33.5 dB and infinite, respectively. Therefore, the obtained PI controller in the FC loop provides the required control parameters.

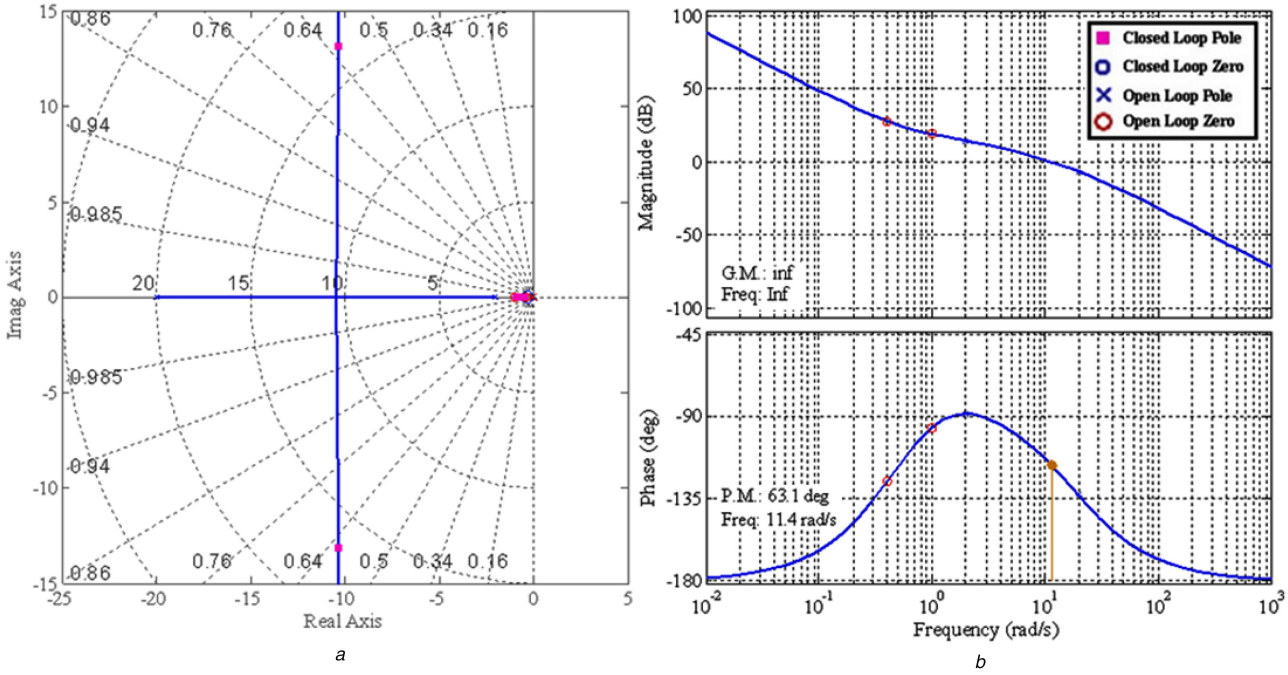

Fig. 4 *DG unit with PI controller and LC*
(a) Root-locus,
(b) Bode plot

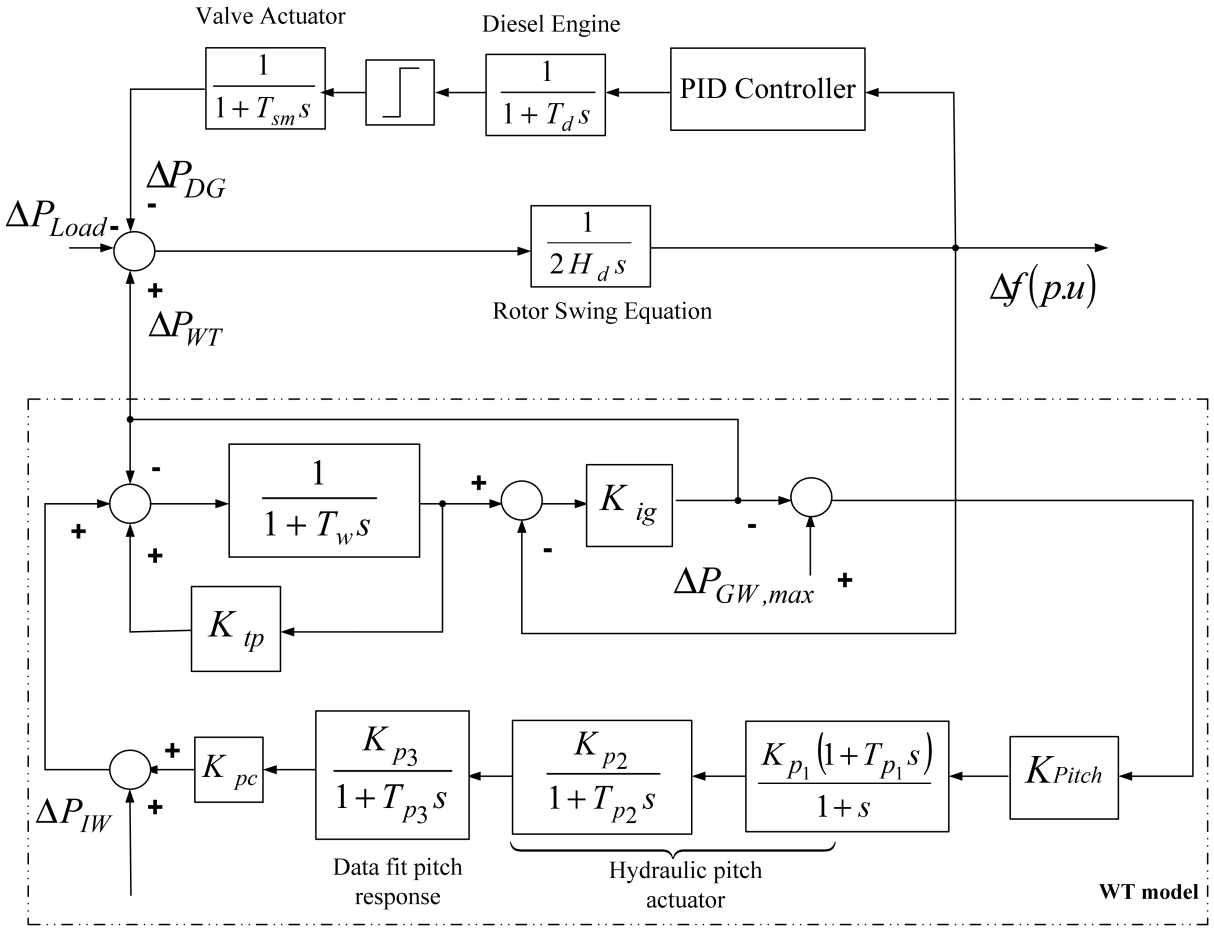

Fig. 5 *Participation of WT with DG unit (DG/WT system)*

5.4 Integration of UC with DG/WT/FC system

The linearised state-space equations of the HMG model are given in [19, 33, 34]. For the given HMG, shown in Fig. 2, the state-space equations are expressed as

$$\Delta\dot{x} = A\Delta x + B\Delta u \tag{7}$$

$$\Delta y = C\Delta x + D\Delta u \tag{8}$$

$$\Delta u = \Delta u_{\mathrm{uc}} = K_{\mathrm{UC}}\Delta u_{\mathrm{in}} \tag{9}$$

where $x = [\Delta P_{\mathrm{F1}}\Delta P_{\mathrm{F2}}\Delta P_{\mathrm{DG}}\Delta H_1\Delta H_2\Delta P_{\mathrm{WT}}\Delta P_{\mathrm{FC}}\Delta f]$ are state variables, $\Delta y = [\Delta f]$ is the output variable, Δf is the frequency

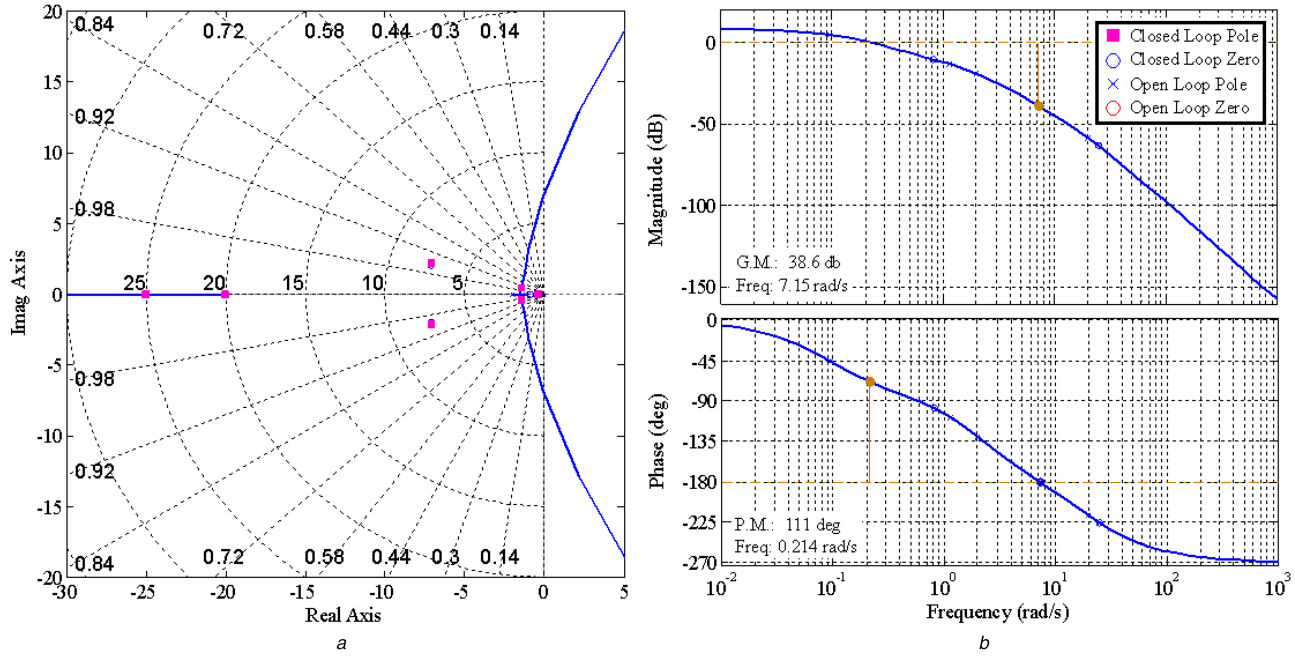

Fig. 6 *Frequency response of the DG/WT system*
(a) Root-locus of the open-loop DG/WT,
(b) Bode plot of the open-loop DG/WT

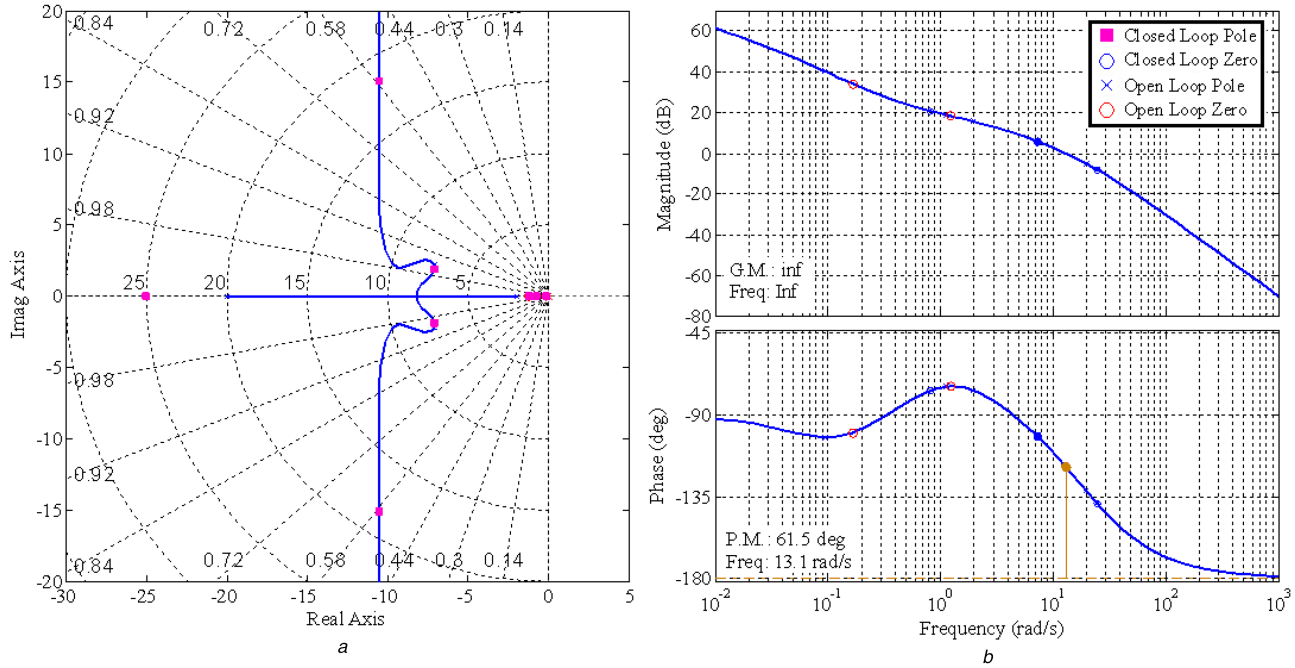

Fig. 7 *Frequency response of the DG/WT system with the PI controller and LC*
(a) Root-locus,
(b) Bode plot

variations, ΔP_{UC} is the output signal of the UC bank, Δu_{uc} is the output signal of UC controller, K_{UC} is the PI controller of the UC bank; and $\Delta u_{in} = \Delta y$ is the feedback input signal of UC controller. The hybrid system formulated in (7) has a single-input, single-output structure. The proposed technique discussed in Sections 2 and 4 is used to design the UC controller (K_{UC}), and the state-space equation shown in (7) is used as the nominal plant $G(s)$. The $G(s)$ transfer function, based on the presented model in Fig. 1, is the DG/WT/FC dynamic models. The feedback function is UC transfer function formulated in (5). Using *linmod* command to obtain $G(s)$ transfer function, the root-locus and bode plot of the hybrid system are obtained as shown in Figs. 9*a* and *b*.

The gain value $K_{P_{UC}} = 57.6$ gives desired damping coefficient, $\zeta = 0.639$. As shown in Fig. 9*b*, the GM and PM are infinite. The open-loop system has two tandem poles at $s = -0.216$ and -0.768. The PI zero with $s = -0.65$ can be placed between the mentioned tandem poles as: $s = (-1/T_{UC}) = -0.65 \Rightarrow T_{UC} = 1.538$. The desired damping coefficient gives: $K_{I_{UC}} T_{UC} = 57.6 \Rightarrow K_{I_{UC}} = 57.6/1.538 = 37.45$.. Therefore, the PI controller is obtained as $K_{UC}(s) = \mathrm{PI}_{UC}(s) = 37.45 \times (((1 + 1.538s)/s))$ with $K_{P_{UC}} = 57.6$ and $K_{I_{UC}} = 37.45$.

As shown in Figs. 9*c* and *d*, the GM, ζ, and PM of the new open-loop system with the obtained PI controller are infinite, 0.639 and 86.4°, respectively. Therefore, the obtained PI controller in the UC control loop provides the required control parameters. According to the obtained results, the PI/PID controller parameters of the HMG subsystems are presented in Table 1.

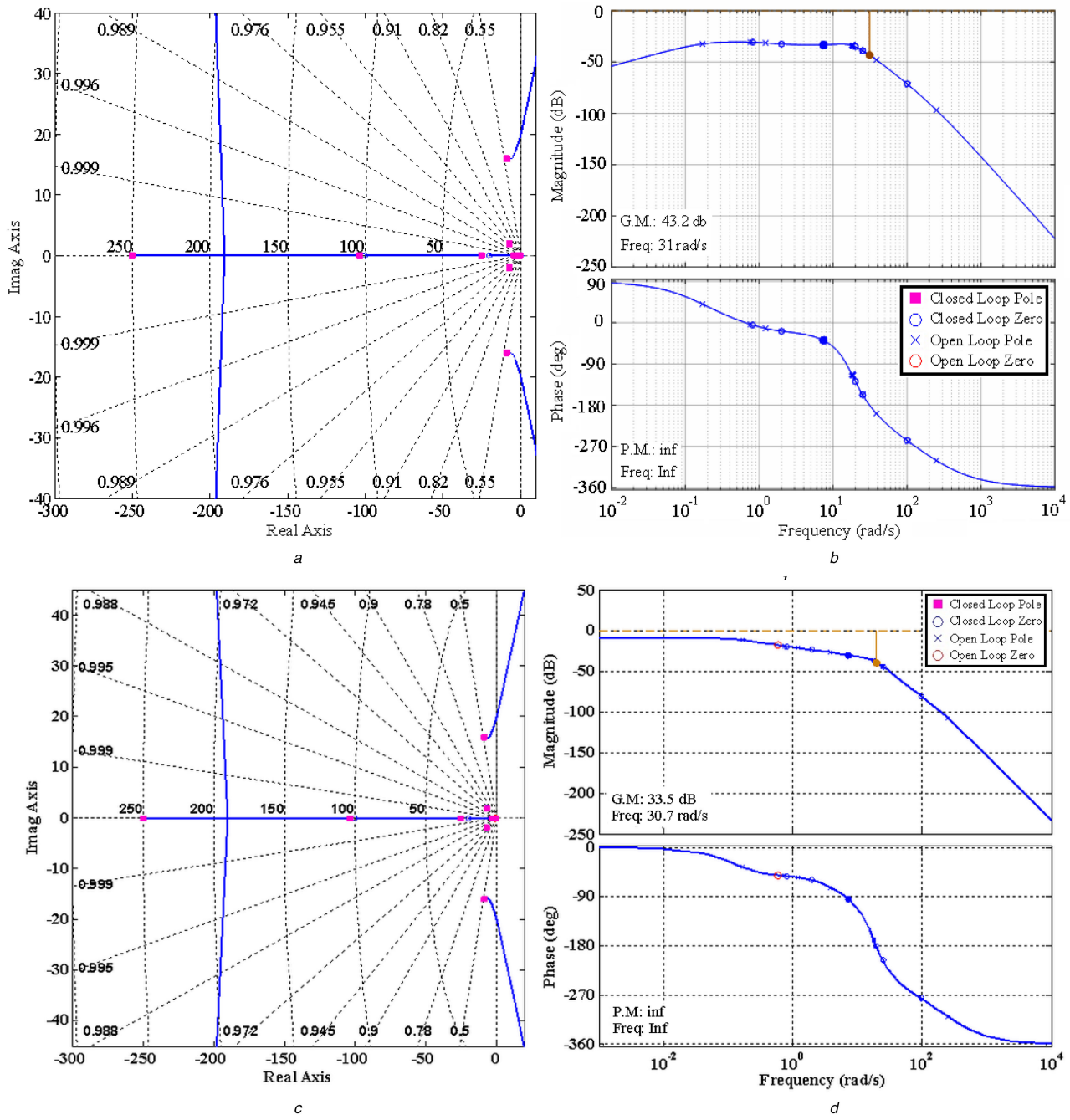

Fig. 8 *Frequency response of the DG/WT/FC system*
(a) Root-locus without PI controller,
(b) Bode plot without PI controller,
(c) Root-locus with PI controller,
(d) Bode plot with PI controller

5.5 FC/UC control parameters using ZN method

In this section, the UC and FC controllers are tuned by ZN method. A detailed study for tuning of the PI/PID controllers using ZN technique is presented in [23, 24, 39]. By using the ZN method, the PI controller parameters are obtained as given in Table 2.

As discussed in Section 5.1, the nominal droop value ($R = 5\%$) is chosen for the DG governor. To remove the DG steady-state error, the integral coefficient is fixed at KIDG = 3. For the WT pitch loop, the proportional controller is selected as $K_{\text{Pitch}} = 272$.

6 Simulation results and discussion

The HMG case study is examined in the face of the load variations and wind power disturbances. In addition, the HMG robustness is verified against system parameter uncertainties. Then, the controller performance and deviations in the system frequency profile are identified and evaluated.

6.1 Time-domain analysis of the islanded HMG

The time-domain frequency variations of the explained hybrid system are examined under different disturbance scenarios. In all simulation results, dashed and solid lines are used instead of ZN and well-tuned controllers, respectively.

Scenario 1(random changes in the load demand and wind power): In this scenario, the performance of designed controllers is estimated under random load and wind power changes as shown in Figs. 10*a* and *b*. Then, the system frequency deviations are recorded for the random load changes and wind power fluctuation as presented in Figs. 10*c* and *d*, respectively.

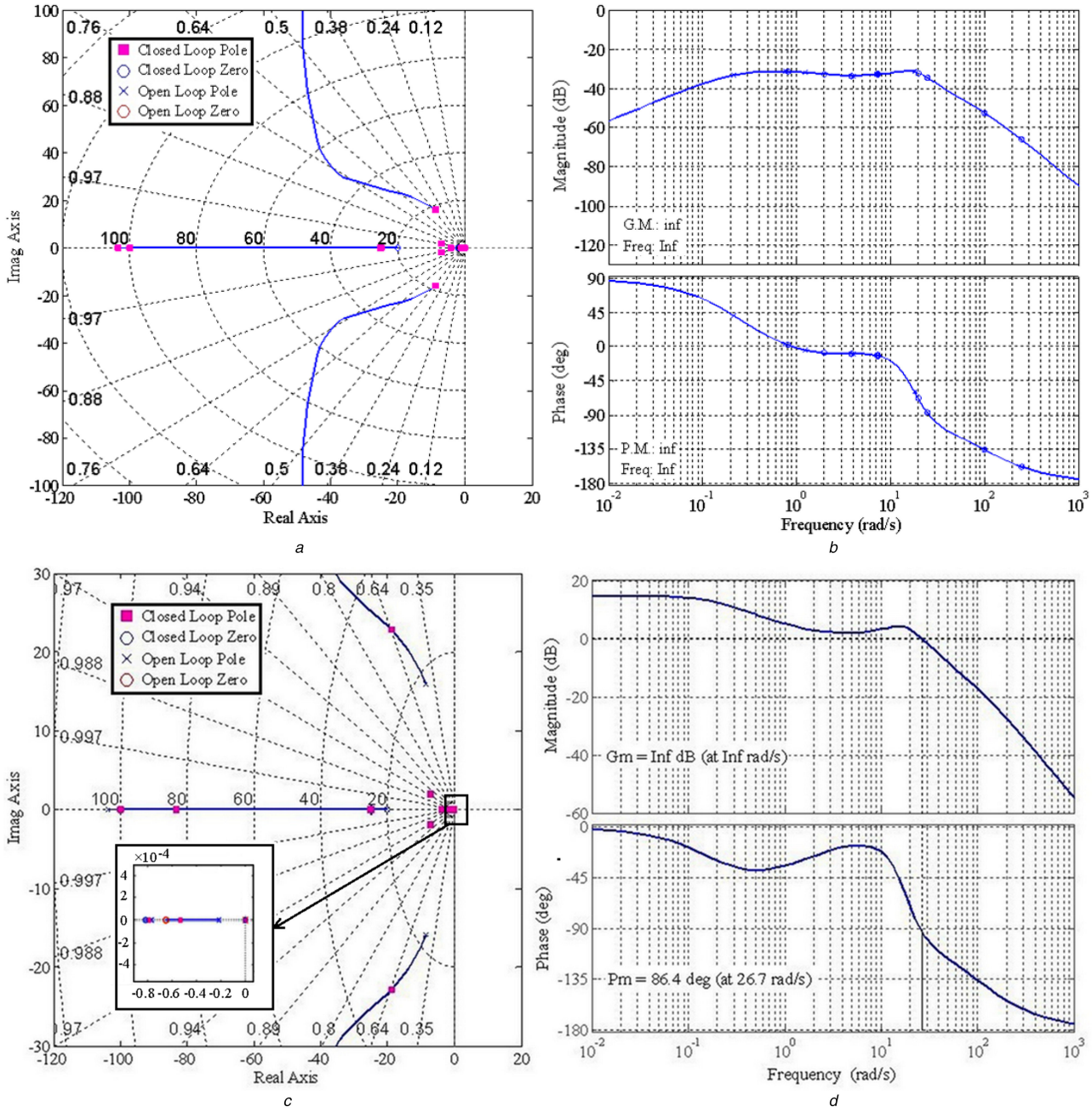

Fig. 9 *Frequency response of the hybrid system with/without PI controller*
(a) Root-locus without PI controller,
(b) Bode plot without PI controller,
(c) Root-locus with PI controller,
(d) Bode plot with PI controller

Table 1 Well-tuned controller parameters

Controller parameters	DG	WT	FC	UC
Proportional coefficient	23	272	3	57.6
Integral coefficient	3	—	1.8	37.45
Derivative coefficient	20	—	—	—

Table 2 ZN controller parameters

Controller parameters	FC	UC
Proportional coefficient	29.79	4.344
Integral coefficient	57.28	3.62

As shown in Figs. 10*c* and *d*, the well-tuned controller minimises the frequency deviations and keeps the system frequency at the nominal value. The low-frequency deviations for the well-tuned controllers are obtained because the UC unit has the ability to keep the power-balancing in the face of transient disturbances, quickly. As well, due to the suitable control conditions for the GM, PM, and ζ, the well-tuned controllers provide better responses than the PI controllers tuned by the ZN method.

Scenario 2 (evaluation of uncertainty): In this section, robustness of the designed controllers is evaluated in the presence of changes in all system parameters up to +35%. For this purpose,

the system frequency deviations for 0.1 p.u. step increase in the load demand are plotted in Figs. 11*a* and *b*.

As shown in Figs. 11*a* and *b*, the well-tuned controllers keep the frequency on the nominal values with low deviations for +35% changes in all parameters and nominal parameters. Due to the desired control conditions mention in Section 2, the well-tuned controllers provide a relatively small undershoot and settling time than the PI controllers tuned by the ZN method. For random disturbances presented in Figs. 10*a* and *b*, the output frequency deviations with ±35% changes in all system parameters are plotted in Figs. 12*a–d*.

As shown in Figs. 12*a–d*, the well-tuned controllers have enough capability to keep the system frequency almost constant in the face of random disturbances and a wide range of parameter variations. Due to the suitable values for the ζ, GM, and PM, the well-tuned controllers keep the system frequency on the nominal value against the wide range of parameter variations and random disturbances, effectively.

To demonstrate the effectiveness of designed controllers, the following frequency variation-based performance index is formulated as

$$\mathrm{ISE}(\Delta f) = \int_0^T |\Delta f(t)|^2 \mathrm{d}t$$

where ISE, $|\Delta f(t)|$, and T are integral of squared error, absolute value of the frequency deviations, and simulation time period, respectively. The ISE indexes are obtained for $T = 30$ s in six different scenarios with random disturbances presented in Figs. 10*a* and *b*. Then, the results are given in Table 3.

The S-1, S-2, and S-3 are the ISE indexes under random load disturbances for nominal parameters,+35%, and −35% changes in all parameters, respectively. The S-4, S-5, and S-6 are ISE indexes under wind power disturbances for nominal parameters, −35% and +35% changes in all parameters, respectively. As shown in Table 3, calculated values for the ISE indexes are quite better when the

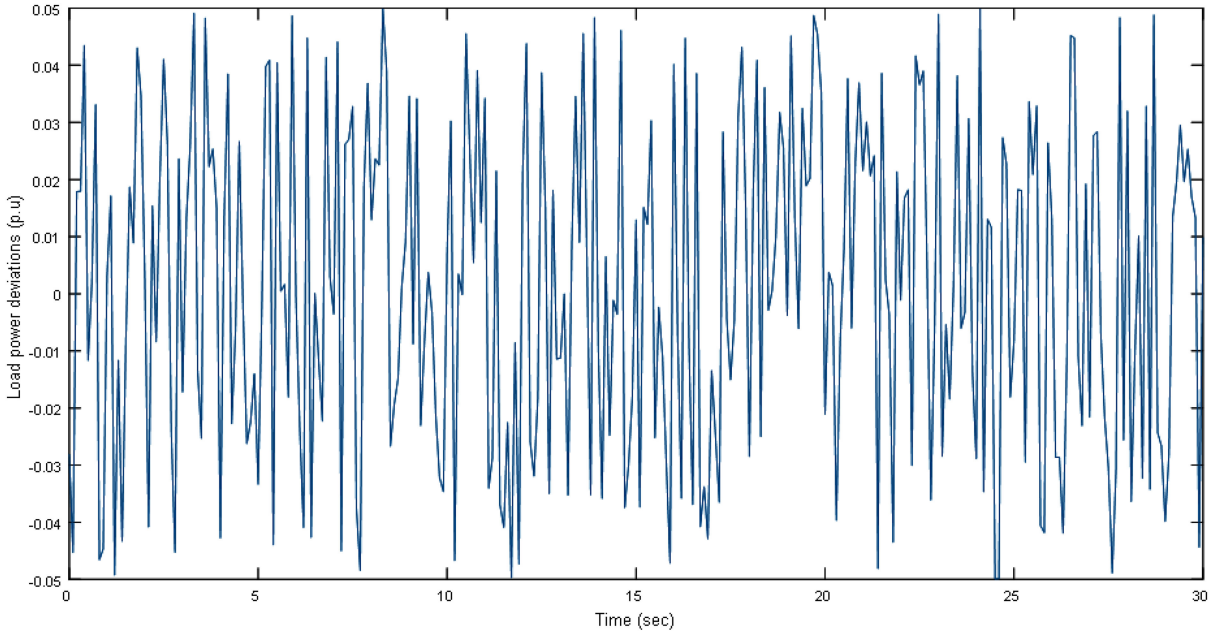

a

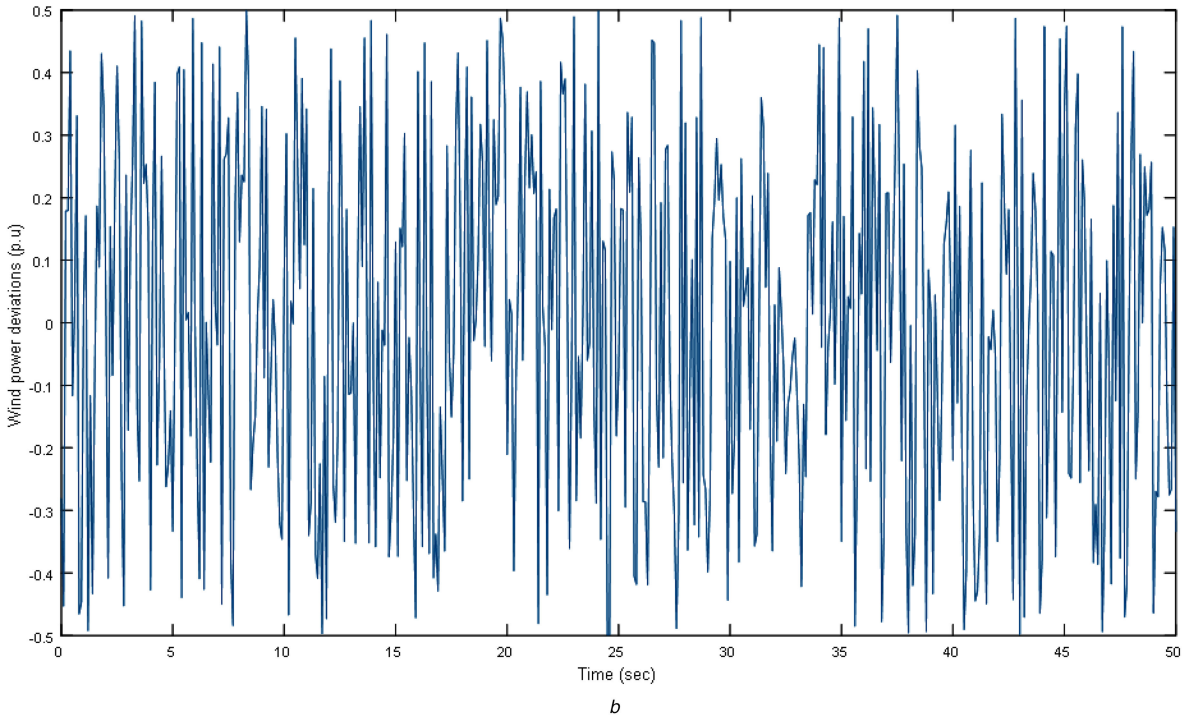

b

Fig. 10 *Continued*

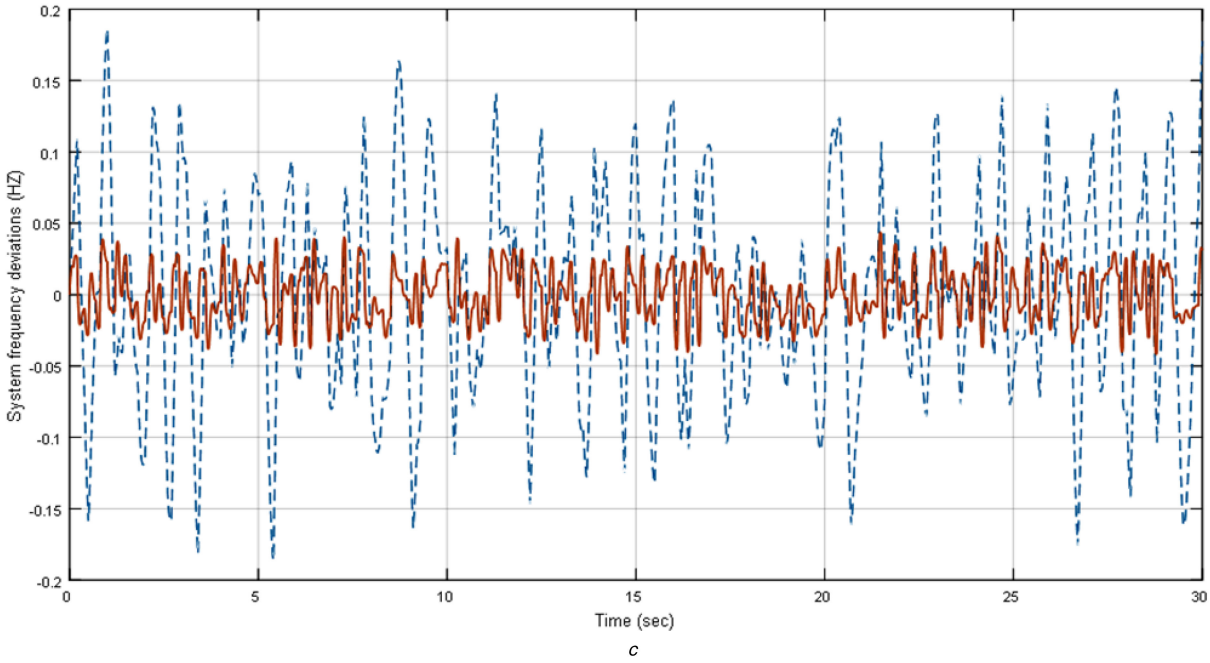

c

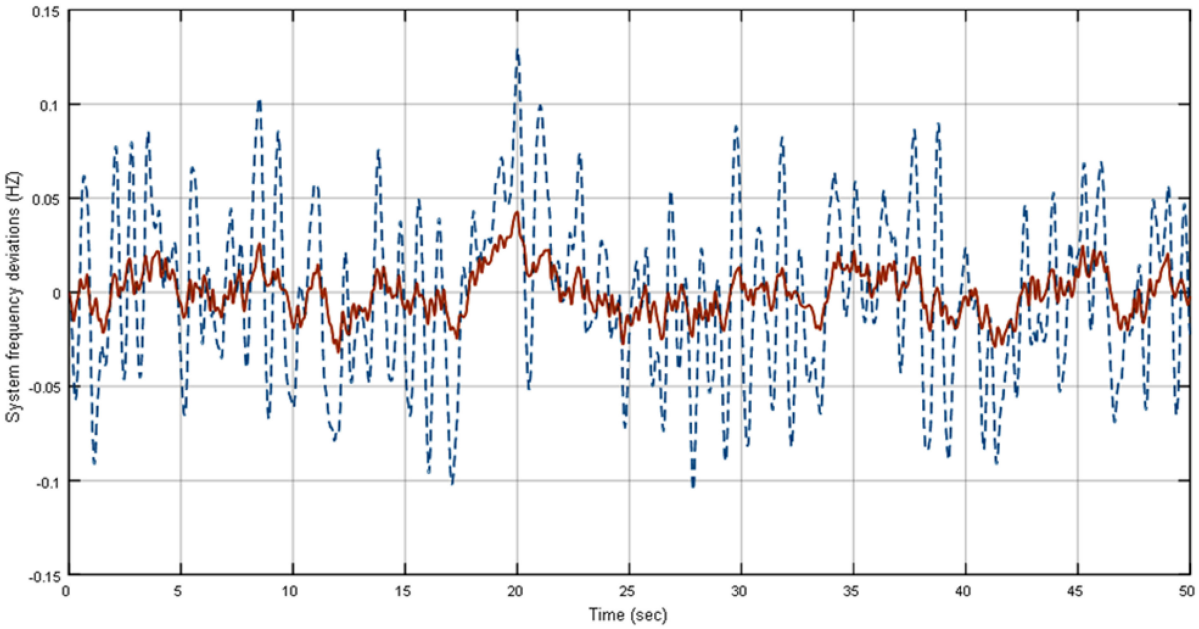

d

Fig. 10 *Random changes in the system inputs and the output frequency deviations*
(a) Random load changes,
(b) Random changes in the wind power,
(c) Frequency deviations for the random load changes,
(d) Frequency deviations for the random changes in the wind power

controller is designed based on the proper values of the GM, PM, and ζ.

Scenario 3 (noise rejection capability): The PI controllers and LC are designed based on the appropriate damping of the system dominant poles. This issue increases the damping of the HMG characteristic equation. Therefore, the system has a sufficient damping and rejects the output noises, quickly. To show this issue, a random noise is applied to the output frequency deviations (Δf), as shown in Figs. 13 and 14*a*. Then, the load frequency deviations are obtained as illustrated in Fig. 14*b*.

As shown in Fig. 14*b*, the proper damping coefficient of the hybrid system damps the influence of output noises, quickly.

6.2 Frequency-domain analysis

The eigenvalues are extremely valuable to ensure the small-signal stability of a hybrid system. They perform a unique set of scalars related with a linear system of equations and can be obtained by the following determinant equation:

$$\det(\lambda[\boldsymbol{I}] - [\boldsymbol{A}]) = 0$$

where $[\boldsymbol{A}]$ is the system matrix, λ is the eigenvalues of a system, and $[\boldsymbol{I}]$ is an identity matrix.

The participation matrix $[\boldsymbol{P}]$ is used to explain the relationship between the state-space variables and the system eigenvalues [19]. For this purpose, the left and right eigenvectors of $[\boldsymbol{A}]$ is combined as a measure to investigate the relationship between state-space variables and eigenvalues. The participation factor P_{ki} shows the influence of the kth state in the ith mode [19]. Through eigenvalue calculation, one can find that the mode k is a mode with low stability margin. The participation matrix $[\boldsymbol{P}]$ is formulated as

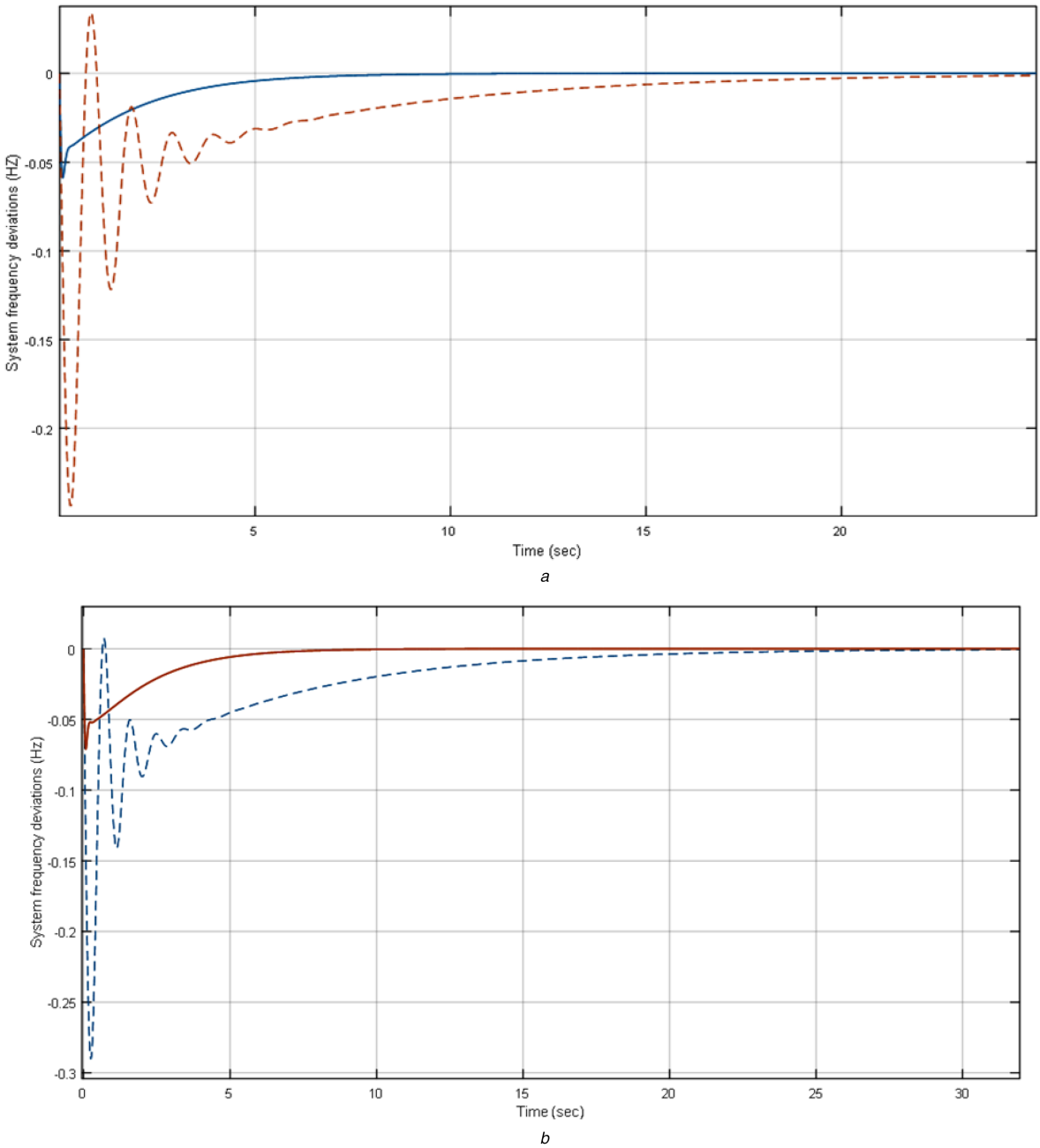

Fig. 11 *Output frequency deviations for a 0.1 p.u. step increase in the load demand*
(a) +35% changes in all HMG parameters,
(b) Output frequency deviations with the system nominal parameters

$$\boldsymbol{P}_i = \begin{bmatrix} P_{1i} \\ P_{2i} \\ . \\ . \\ P_{ki} \end{bmatrix} = \begin{bmatrix} \phi_{1i}\varphi_{i1} \\ \phi_{2i}\varphi_{i2} \\ . \\ . \\ \phi_{ki}\varphi_{ik} \end{bmatrix} \tag{10}$$

where φ_{ki} is the kth element of the right eigenvector $\boldsymbol{\varphi}_i$. As well, it is the entry on the kth row and ith column of the modal matrix $[\boldsymbol{\varphi}]$. ϕ_{ki} is the kth element of the left eigenvector $\boldsymbol{\phi}_i$. In addition, it is the element on the ith row and kth column of the modal matrix $[\boldsymbol{\phi}]$ [19].

According to the state-space equations of the hybrid system presented in (7), the system eigenvalues are obtained as shown in Table 4. The presented eigenvalues belong to the total transfer function of the hybrid system. The HMG subsystems, like DG, FC, WT, and UC, influence on the system eigenvalues. Therefore, the obtained eigenvalues are classified based on related subsystem dependency, as shown in Table 4. This classification is performed by disconnecting of the considered subsystem from the HMG, while other subsystems participate in the power-sharing. By disconnecting of each subsystem, related eigenvalues are not visible in the obtained results.

According to the obtained results, the well-tuned controllers change the location of dominant complex eigenvalues to the left side of the s-plane and enhance the system damping and the stability margin of the hybrid system. As discussed in Sections 5.1 and 5.2, the DG without LC has lower stability margin. With and without UC, the designed LC in the DG governor loop dramatically increases the damping of the DG eigenvalues to 0.63 and 0.47, respectively. This improvement of the DG stability margin directly enhances the overall stability and performance of the hybrid system.

6.3 Comparing the presented method with intelligent approaches

In [5], a new online intelligent method by the combination of the fuzzy logic and PSO methods are used to control the output

frequency of the HMG. Then, the step response of the hybrid system for 0.1 p.u. load increase is obtained. According to the presented results, the fuzzy and PSO-fuzzy controllers have the damped-oscillatory and fast-damped responses with settling times about 4 and 1 s, respectively. The maximum frequency undershoot is also obtained about −0.06 p.u. for both cases. By replacing a PI controller and the LC instead of the intelligent controller and using the presented approach discussed in Sections 2 and 4, the new controller parameters are obtained as $(0.41 + 17.52/s) \times (s + 17.16)$. This function is equal to the PID controller with $K'_{P_{DG}} = 24.56$, $K'_{I_{DG}} = 300.6$, and $K'_{D_{DG}} = 0.41$. The root-locus and bode plot of the HMG with the designed controller in the feedback loop are obtained as shown in Figs. 15*a* and *b*. According to Figs. 15*a* and *b*, the GM, PM, and ζ are infinite, 53.7° and 0.5, respectively. Therefore, designed controller satisfies the required control conditions discussed in Section 2. For the obtained controller, the frequency deviation in the face of 0.1 p.u. load increase is obtained as illustrated in Fig. 15*c*. The maximum undershoot is about −0.033 p.u. and the settling time is about 0.75 s. Therefore, the PI/LC demonstrates a better performance than the fuzzy/PSO and fuzzy controllers in terms of settling time and undershoot characteristics.

7 Conclusion

The HMG may consist of numerous decentralised power providers. Thus, coordination among those subsystems using an effective technique is necessary. The presented controllers and compensators are tuned based on the proper values of the GM, PM, ζ, and coordination of the HMG subsystems. The control targets for the presented approach are providing of fast system response with enough relative stability.

The designed controllers are examined under different step, random, and noise disturbances. According to the obtained results, the well-tuned conventional controllers have desired control specifications such as robustness, small overshoot/undershoot, and low settling time. The proposed controllers enhance the relative stability of the HMG subsystems and provide a better performance than intelligent controllers in terms of settling time and overshoot/undershoot. The obtained results are also supported by eigenvalue analysis and the ISE indexes.

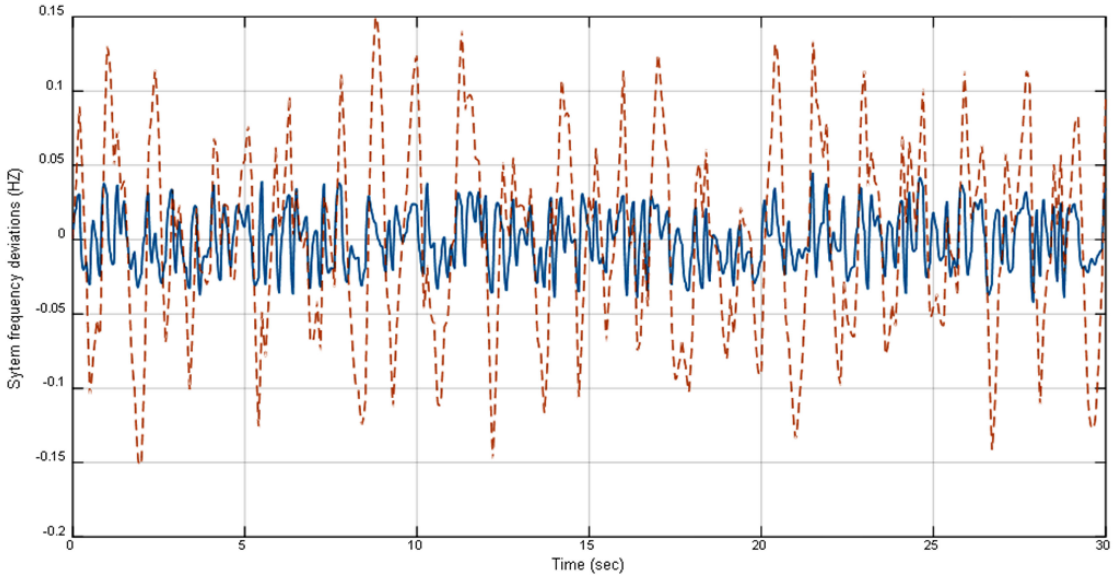

a

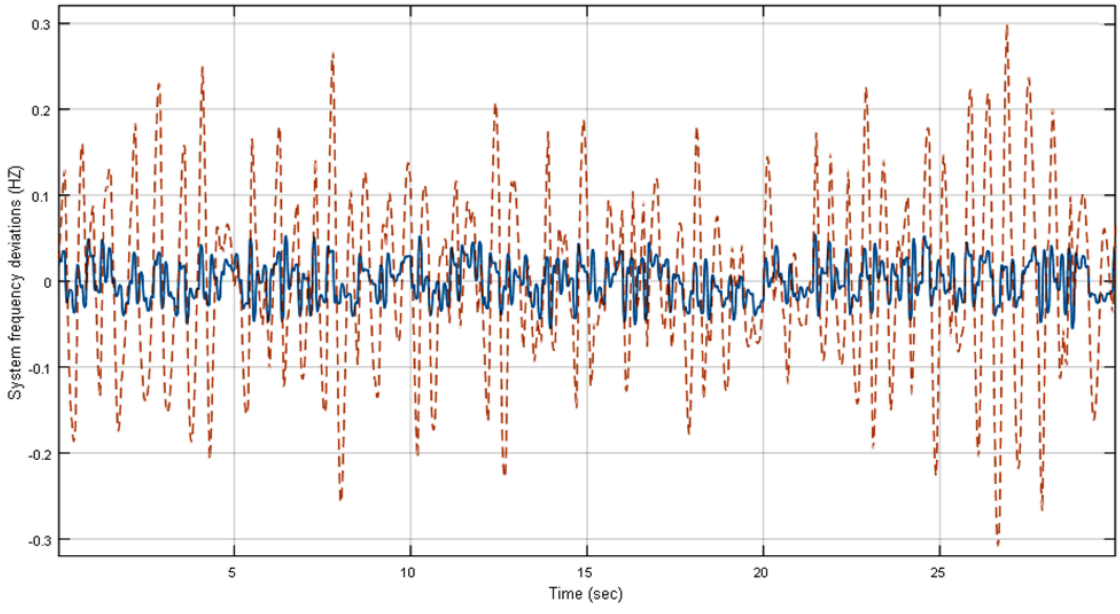

b

Fig. 12 *Continued*

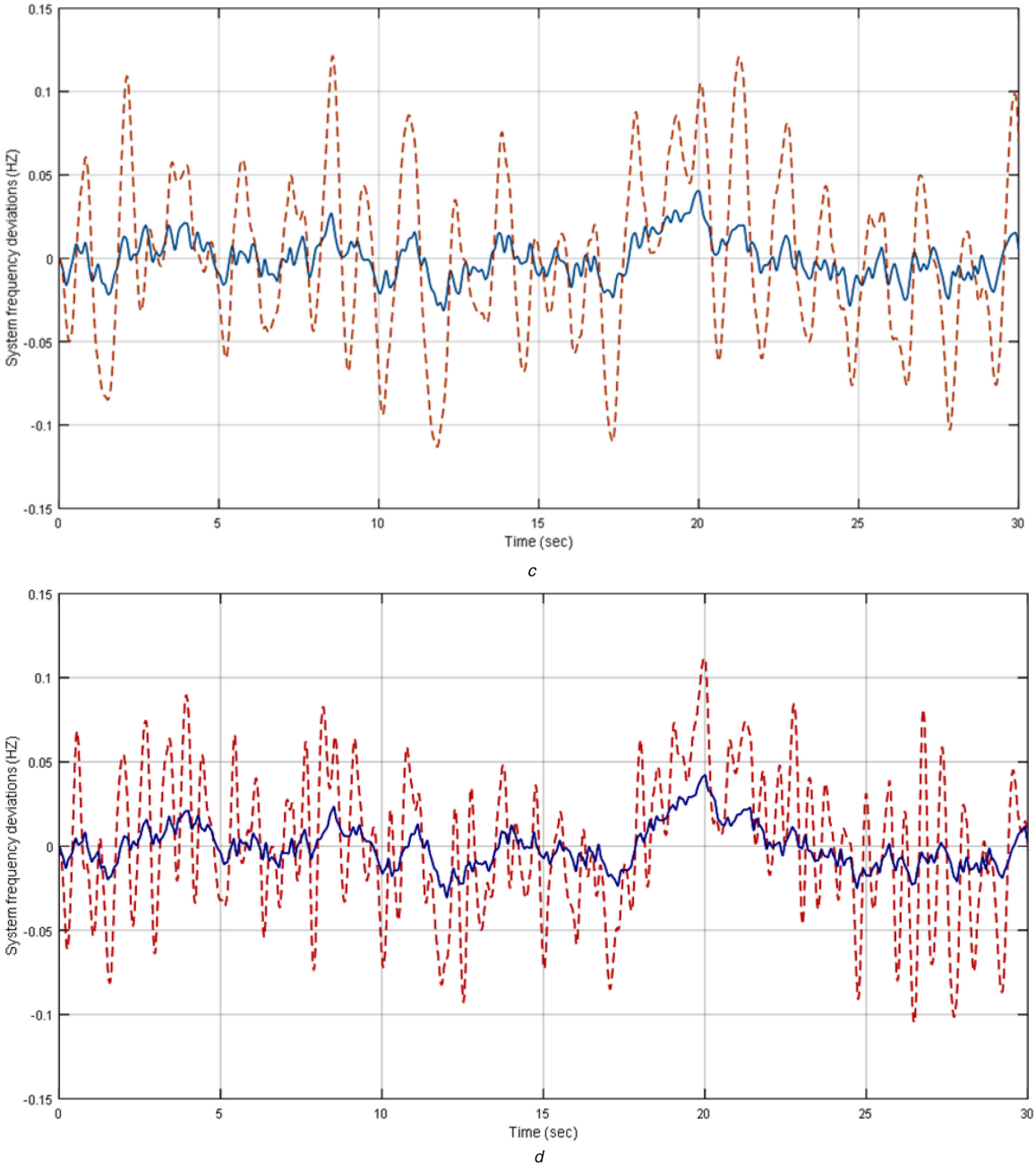

Fig. 12 *Output frequency deviations for ±35% changes in the all system parameters and input random disturbances*
(a) +35% parameter changes with the random load changes,
(b) −35% parameter changes with the random load changes,
(c) +35% parameter changes with the random changes in the wind power,
(d) −35% parameter changes with the random changes in the wind power

Table 3 ISE index for different scenarios

Scenario	ZN controller	Well-tuned controller
S-1	0.15	10e−3
S-2	0.25	8.2e−3
S-3	0.12	10.6e−3
S-4	0.061	4.95e−3
S-5	0.0526	4.73e−3
S-6	0.075	4.67e−3

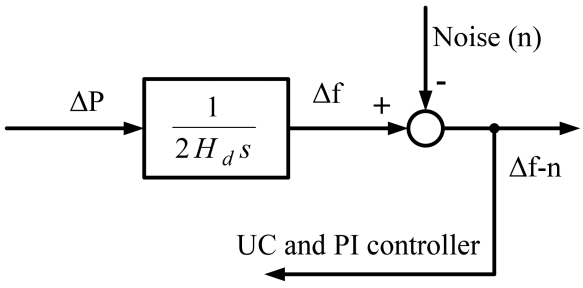

Fig. 13 *Appling of noise in the system output*

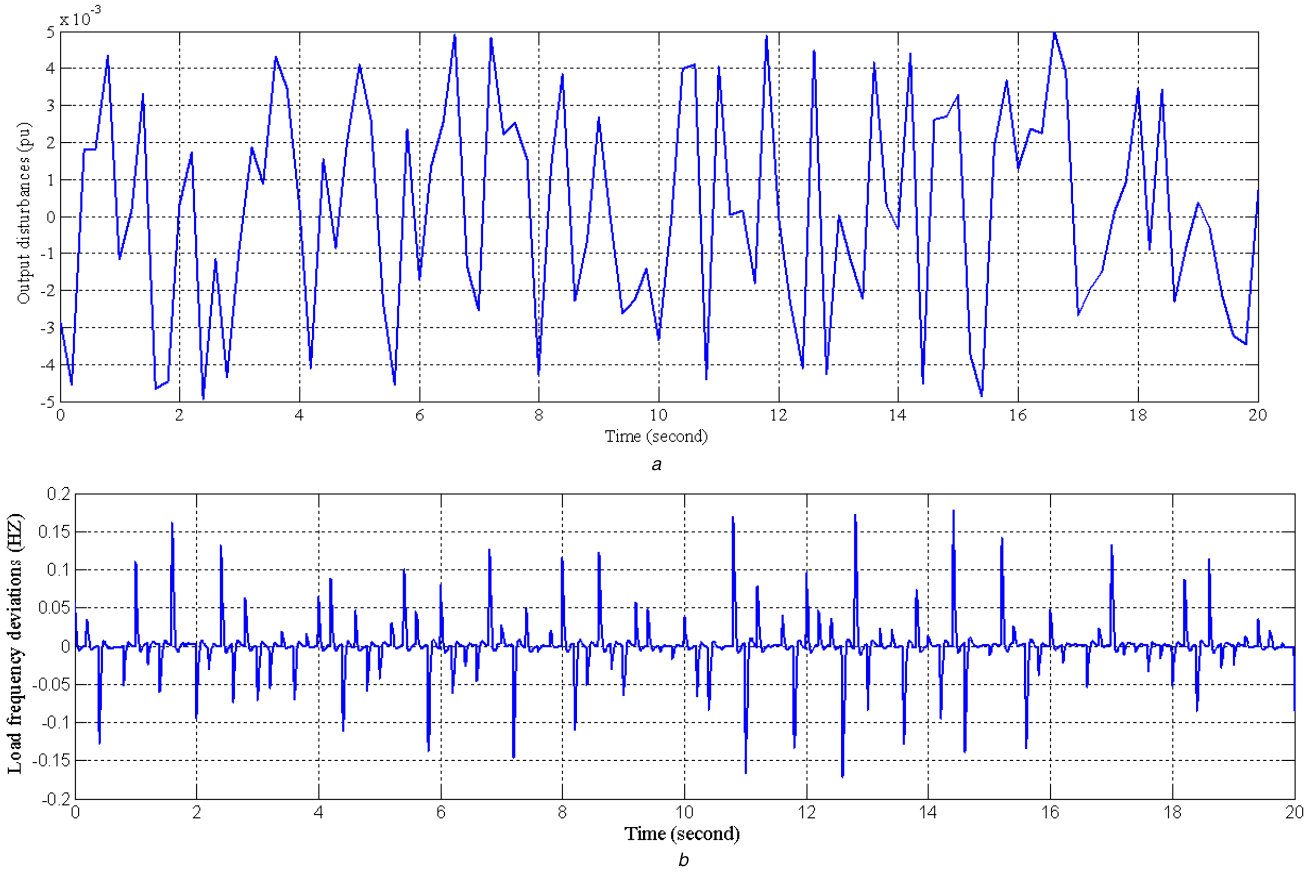

Fig. 14 *Output noise and load frequency deviations*
(a) Noise signal variations (p.u.),
(b) Output frequency deviations (Hz)

Table 4 Eigenvalues of the hybrid system

Eigenvalues	ZN controllers		Well-tuned controllers	
	with UC	without UC	with UC	without UC
$\lambda_{1,\,2,3}$ (DG)	−98.53,−1.39 ± 7.12i, $\zeta = 0.19$	−26.88,−0.75 ± 6.8i, $\zeta = 0.11$	−83.13,−18.57 ± 22.8i, $\zeta = 0.63$	−103.7,−8.56 ± 15.92i, $\zeta = 0.47$
$\lambda_{4,5,6}$ (WT)	−7.05 ± 2.05i, $\zeta = 0.96$,−0.167	−7.05 ± 2.04i, $\zeta = 0.96$,−0.11	−7.07 ± 1.96i, $\zeta = 0.96$,−0.787	−7.08 ± 1.93i, $\zeta = 0.96$,−0.77
λ_7 (Δf)	−2.48	−0.8	−100	−1.26
λ_8 (FC)	−0.8	−2.49	−3.94	−4.01
λ_9 (UC)	−98.53	—	−1.56	—

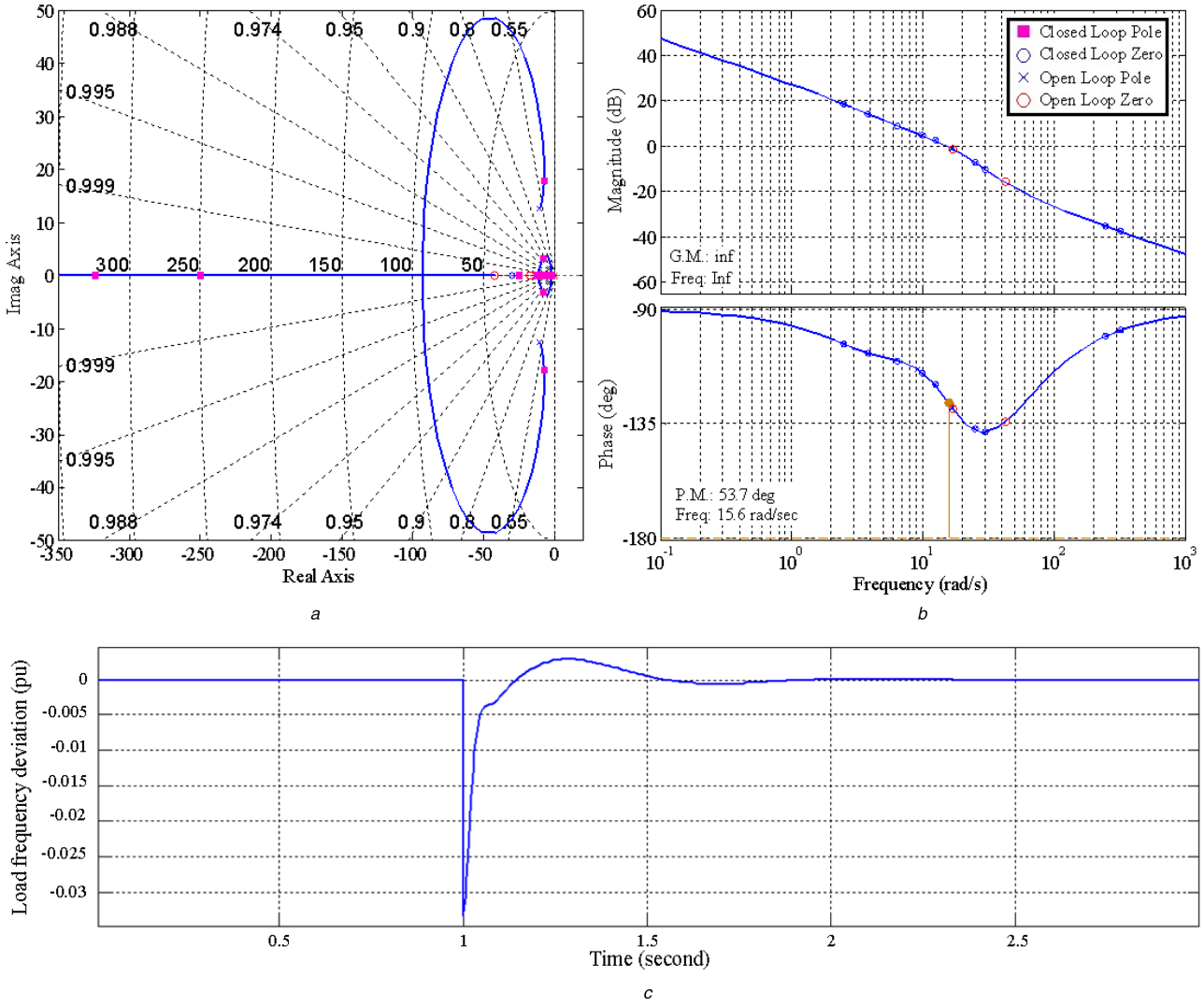

Fig. 15 *Frequency and step responses of the hybrid system*

(a) Root-locus of the hybrid system with PI controller and LC,

(b) Bode plot of the hybrid system with PI controller and LC,

(c) The load frequency deviation for 0.1 (p.u.) step increase in the load demand

8 References

[1] Eto, J., Lasseter, R., Schenkman, B., *et al.*: Overview of the CERTS microgrid laboratory test bed. 2009 CIGRE/IEEE PES Joint Symp. Integration of Wide-Scale Renewable Resources into the Power Delivery System, 2009

[2] Lasseter, R., Akhil, A., Marnay, C., *et al.*: 'The CERTS microgrid concept'. White paper for Transmission Reliability Program, Office of Power Technologies, US Department of Energy, 2002, vol. 2, issue 3, p. 30

[3] Lasseter, R.H., Eto, J., Schenkman, B., *et al.*: 'CERTS microgrid laboratory test bed', *IEEE Trans. Power Deliv.*, 2011, **26**, (1), pp. 325–332

[4] Nichols, D.K., Stevens, J., Lasseter, R.H., *et al.*: 'Validation of the CERTS microgrid concept the CEC/CERTS microgrid testbed'. Power Engineering Society General Meeting, 2006, 2006

[5] Bevrani, H., Habibi, F., Babahajyani, P., *et al.*: 'Intelligent frequency control in an AC microgrid: online PSO-based fuzzy tuning approach', *IEEE Trans. Smart Grid*, 2012, **3**, (4), pp. 1935–1944

[6] Mahmood, H., Michaelson, D., Jiang, J.: 'Decentralized power management of a PV/battery hybrid unit in a droop controlled islanded microgrid', *IEEE Trans. Power Electron.*, 2015, **30**, (12), pp. 7215–7229

[7] Sachs, J., Sawodny, O.: 'A two-stage model predictive control strategy for economic diesel-PV-battery island microgrid operation in rural areas', *IEEE Trans. Sust. Energy*, 2016, **7**, (3), pp. 903–913

[8] Pathak, G., Singh, B., Panigrahi, B.K.: 'Control of wind-diesel microgrid using affine projection-like algorithm', *IEEE Trans. Ind. Inf.*, 2016, **12**, (2), pp. 524–531

[9] Sekhar, P., Mishra, S., Sharma, R.: 'Data analytics based neuro-fuzzy controller for diesel-photovoltaic hybrid AC microgrid', *IET Gener. Transm. Distrib.*, 2015, **9**, (2), pp. 193–207

[10] Dou, C., Zhang, Z., Yue, D., *et al.*: 'Improved droop control based on virtual impedance and virtual power source in low-voltage microgrid', *IET Gener. Transm. Distrib.*, 2016, **11**, pp. 1046–1054

[11] Patterson, M., Macia, N.F., Kannan, A.M.: 'Hybrid microgrid model based on solar photovoltaic battery fuel cell system for intermittent load applications', *IEEE Trans. Energy Convers.*, 2015, **30**, (1), pp. 359–366

[12] Eghtedarpour, N., Farjah, E.: 'Power control and management in a hybrid AC/DC microgrid', *IEEE Trans. Smart Grid*, 2014, **5**, (3), pp. 1494–1505

[13] Bevrani, H., Feizi, M.R., Ataee, S.: 'Robust frequency control in an islanded microgrid: H∞ and μ-synthesis approaches', *IEEE Trans. Smart Grid*, 2016, **7**, (2), pp. 706–717

[14] Kunusch, C., Puleston, P., Mayosky, M.: 'Control-oriented modeling and experimental validation of a PEMFC generation system', *IEEE Trans. Energy Convers.*, 2011, **26**, (3), pp. 851–861

[15] Zhu, X., Li, X., Shen, G., *et al.*: 'Design of the dynamic power compensation for PEMFC distributed power system', *IEEE Trans. Ind. Electron.*, 2010, **57**, (6), pp. 1935–1944

[16] Pukrushpan, J.T., Stefanopoulou, A.G., Peng, H.: '*Control of fuel cell power systems: principles, modeling, analysis and feedback design*' (Springer Science & Business Media, 2004)

[17] Nayeripour, M., Hoseintabar, M., Niknam, T.: 'Frequency deviation control by coordination control of FC and double-layer capacitor in an autonomous hybrid renewable energy power generation system', *Renew. Energy*, 2011, **36**, (6), pp. 1741–1746

[18] Inthamoussou, F.A., Pegueroles-Queralt, J., Bianchi, F.D.: 'Control of a supercapacitor energy storage system for microgrid applications', *IEEE Trans. Energy Convers.*, 2013, **28**, (3), pp. 690–697

[19] Singh, V.P., Mohanty, S.R., Kishor, N., *et al.*: 'Robust H-infinity load frequency control in hybrid distributed generation system', *Int. J. Electr. Power Energy Syst.*, 2013, **46**, pp. 294–305

[20] Kamel, R.M., Chaouachi, A., Nagasaka, K.: 'Enhancement of micro-grid performance during islanding mode using storage batteries and new fuzzy logic pitch angle controller', *Energy Convers. Manage.*, 2011, **52**, (5), pp. 2204–2216

[21] Kakigano, H., Miura, Y., Ise, T.: 'Distribution voltage control for dc microgrids using fuzzy control and gain-scheduling technique', *IEEE Trans. Power Electron.*, 2013, **28**, (5), pp. 2246–2258

[22] Sa-ngawong, N., Ngamroo, I.: 'PSO-based Sugeno fuzzy logic controller of photovoltaic generator for frequency stabilization in stand-alone power

system'. 2013 IEEE PES Asia-Pacific Power and Energy Engineering Conf. (APPEEC), 2013
[23] Ogata, K., Yang, Y.: '*Modern control engineering*' (Prentice-Hall, New Jersey, 1970)
[24] Kwakernaak, H., Sivan, R.: '*Linear optimal control systems*' (Wiley-Interscience, New York, 1972), vol. 1
[25] Kuo, B.C.: '*Automatic control systems*' (Prentice Hall PTR, New Jersey, 1987)
[26] Bevrani, H.: '*Robust power system frequency control*' (Springer, Boston, 2014)
[27] Bhatti, T., Al-Ademi, A., Bansal, N.: 'Load frequency control of isolated wind diesel hybrid power systems', *Energy Convers. Manage.*, 1997, **38**, (9), pp. 829–837
[28] Tripathy, S., Kalantar, M., Balasubramanian, R.: 'Dynamics and stability of wind and diesel turbine generators with superconducting magnetic energy storage unit on an isolated power system', *IEEE Trans. Energy Convers.*, 1991, **6**, (4), pp. 579–585
[29] Scott, G., Wilreker, V., Shaltens, R.: 'Wind turbine generator interaction with diesel generators on an isolated power system', *IEEE Trans. Power Appar. Syst.*, 1984, **PAS-103**, (5), pp. 933–937
[30] Nacfaire, H.: '*Wind-diesel and wind autonomous energy systems*' (CRC Press, Mykonos, Greece, 1989)
[31] Kariniotakis, G., Stavrakakis, G.: 'A general simulation algorithm for the accurate assessment of isolated diesel-wind turbines systems interaction. Part II: implementation of the algorithm and case-studies with induction generators', *IEEE Trans. Energy Convers.*, 1995, **10**, (3), pp. 584–590
[32] Stavrakakis, G., Kariniotakis, G.: 'A general simulation algorithm for the accurate assessment of isolated diesel-wind turbines systems interaction. Part I: A general multimachine power system model', *IEEE Trans. Energy Convers.*, 1995, **10**, (3), pp. 577–583
[33] Tripathy, S.: 'Dynamic simulation of hybrid wind-diesel power generation system with superconducting magnetic energy storage', *Energy Convers. Manage.*, 1997, **38**, (9), pp. 919–930
[34] An, C.S., Hashiguchi, T., Goda, T.: 'Control scheme of hybrid wind-diesel power generation system', in Krause, G. (Ed.): '*From turbine to wind farms – technical requirements and spin-off products*' (InTech, India, 2011)
[35] Papathanassiou, S.A., Papadopoulos, M.P.: 'Dynamic characteristics of autonomous wind–diesel systems', *Renew. Energy*, 2001, **23**, (2), pp. 293–311
[36] Tan, W., Zhang, J.: 'Load frequency control for wind-diesel hybrid systems'. 2011 30th Chinese Control Conf. (CCC), 2011
[37] Bevrani, H.: '*Robust power system frequency control*' (Springer, New York, 2009), vol. 85
[38] Bevrani, H., Ise, T.: '*Microgrid dynamics and control*' (John Wiley & Sons, New Jersey, 2017)
[39] Bevrani, H., Ghosh, A., Ledwich, G.: 'Renewable energy sources and frequency regulation: survey and new perspectives', *IET Renew. Power Gener.*, 2010, **4**, (5), pp. 438–457

9 Appendix

Total load demand = 1000 kW (1 p.u.)

Diesel generator:

Rated power = 500 kW, $H_d = 1.5$, $T_d = 0.5$(s), $T_{sm} = 0.05$(s), $f = 60$(Hz)Wind turbine:

Rated power = 500 kW-AC, $T_w = 4\ s$, $K_{pc} = 0.08$, $K_{p1} = 1.25$, $K_{p2} = 1$, $K_{p3} = 1.4$, $K_{ig} = 1.494$, $T_{p1} = 0.6\ s$, $T_{p2} = 0.041\ s$, $T_{p3} = 1\ s$, $K_{tp} = 0.004$,

Ultracapacitor:

Rated power = 200 kW, $T_{UC} = 0.01\ s$,Fuel cell:(4 units, 100 kW each) = 400 kW, $T_{ln} = 0.04\ s$, $T_{IC} = 0.004\ s$ $T_{fc} = 0.26\ s$,